

Investigation of Sodium Doped Lanthanum Manganite in Optical, Dielectric and Capacitive Perspective Prepared by Flux Method

R. Majumder^{1*}, M. A. R. Sarker², M. M. Hossain³, M. E. Hossain¹, D. Shen¹, A. K. M. S. Reza², M. H. Kabir²

¹Physics Discipline, Khulna University, Khulna 9208, Bangladesh

²Department of Physics, University of Rajshahi, Rajshahi 6205, Bangladesh

³Industrial Physics Division, BCSIR Laboratories Dhaka, BCSIR, Dhaka 1205, Bangladesh

Received 24 December 2018, accepted in final revised form 18 March 2019

Abstract

A comprehensive analysis of optical and dielectric properties of a material is very much essential for the research of device fabrication. From this perception, the sodium (Na) doped lanthanum manganite with 15% substitution of La by Na ($\text{La}_{0.85}\text{Na}_{0.15}\text{MnO}_3$) has been synthesized using the flux method and investigated to observe the optical absorbance, refractive index, capacitance and dielectric constant. In this study, we have reported better optical absorbance for the monovalent Na doping with a slightly lower value of the energy band gap (~ 1.57 eV) compared to the divalent Sr doping on parent LaMnO_3 . The structural analysis has been accomplished using X-ray diffraction (XRD) and Fourier transform infrared spectroscopy (FTIR) to confirm the ability of the flux method to grow higher order $\text{La}_{0.85}\text{Na}_{0.15}\text{MnO}_3$ crystal satisfactorily. Optical properties of $\text{La}_{0.85}\text{Na}_{0.15}\text{MnO}_3$ have been estimated using UV-Vis spectroscopy and the frequency dependent electronic properties (ac conductivity, dielectric constants and capacitance) have been investigated using a precision impedance analyzer. The capacitance has been reported in Pico farad range for $\text{La}_{0.85}\text{Na}_{0.15}\text{MnO}_3$ crystal with the low value of dielectric constant throughout the high-frequency region.

Keywords: $\text{La}_{0.85}\text{Na}_{0.15}\text{MnO}_3$; Flux method; Optical properties; Dielectric properties.

© 2019 JSR Publications. ISSN: 2070-0237 (Print); 2070-0245 (Online). All rights reserved.
doi: <http://dx.doi.org/10.3329/jsr.v11i2.39351> J. Sci. Res. **11** (2), 195-207 (2019)

1. Introduction

The lanthanum manganite system doped with alkaline earth metals are widely recognized as cathode materials in a high-temperature solid oxide fuel cell (SOFC) [1] and their colossal-magneto resistance (CMR) effect near the Curie temperature T_C is important in device applications [2]. Hence, over the few decade's oxygen stoichiometry [3,4], catalytic activity for oxygen reduction [5,6], strong electron-phonon interaction [7], charge and orbital ordering [8], electrical conductivity [9] and many other important properties of these materials have been extensively studied for divalent cation (Ca, Sr, Ba etc.)-doping.

* Corresponding author: rinkumajumder02@gmail.com

Investigation of monovalent Na doping on lanthanum manganite system has been started recently [10-16]. Introducing metal (divalent or monovalent) doping on parent antiferromagnetic LaMnO_3 , for a certain doping content ferromagnetic transition is achieved with the formation of metallic phases with a fully spin-polarized conduction band [17]. These interesting and unusual changes can be described by the Zener double exchange (ZDE) mechanism [18]. An amount $2x$ of Mn^{3+} is transmuted to Mn^{4+} for every amount x of Na doping. Hence, even for a small amount of Na doping, a large number of carriers (holes) are achieved with the increased conductivity [10]. The same amount of monovalent Na doping in parent LaMnO_3 can produce double hole density than the calcium or strontium doping. Hence, it is possible to get an equal amount of hole doping by substituting a lower amount of cation substitution for Na compared to the Ca or Sr-doped manganites [14]. The hole-doped manganite or the electron-doped manganite undergoes an insulator-to-metal transition behaves like a polaronic semiconductor [19]. Moreover, Na-doped lanthanum manganites have large T_c as well as large magnetoresistance values near room temperature which nominates this compound as encouraging materials for information technologies, medicine, and low-temperature thermal engineering [12]. Hence, it is desirable to study this promising material at the different point of views for its numerous industrial applications and research for device fabrication. To the best of our knowledge the optical, dielectric and capacitive properties of the sodium-doped lanthanum manganite have not been studied extensively in the previously existing literature. Hence, in our present study, we are motivated to investigate the optical absorbance, optical energy band gap, refractive index, dielectric constant and capacitance of this reliable material, important in semiconducting, optical and electrical nature identification perception. Ehi-Eromosele *et al.* [12] have got the highest crystallinity for $x=0.15$ in their observation. So in our present study, the value of doping content x ($x=0.15$) has been chosen to ensure high crystallinity of the sample. There are large numbers of techniques to grow crystalline structure all over the world. Among all, one of the most common and easier technique is the solid-state reaction technique. But the major problem for conventional solid-state reaction technique to grow Na-doped lanthanum manganite is the loss of Na during sintering process [11,12]. Moreover, the origination of dirt, impurity, defect and thermal strain during long sintering process can occur in the solid-state reaction technique. Defect, impurity, dirt, and strain can directly affect the optical properties such as optical band gap, optical absorbance etc. By using the flux material together with our target compound can protect dirt, impurities, and oxides away from the surface of the molten composite material. It acts as if there were a vacuum container surrounding the molten material. Therefore, protects the molten material from further contamination of crucible or other impurities originate during long sintering process and minimize the loss of Na due to oxidation. Hence, to provide a clean environment for the crystal growth with fewer defects and less thermal strain, we have used flux method taking NaCl salt as flux material incorporated with the conventional solid-state reaction which is used widely all over the world [20-23].

2. Materials and Method

2.1. Sample preparation

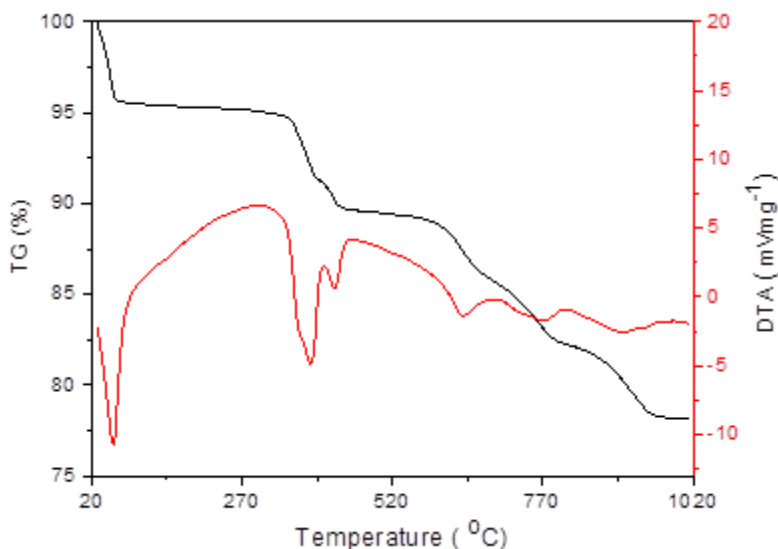


Fig. 1. The TG/DTA curves for the phase formation and thermal decomposition of $\text{La}_{0.85}\text{Na}_{0.15}\text{MnO}_3$ sample.

High-purity (>99.9%) powders of La_2O_3 , NaCl and MnO_2 were used as the starting materials for the preparation of $\text{La}_{0.85}\text{Na}_{0.15}\text{MnO}_3$ sample using flux method. Initially, we have studied the phase formation with the help of thermal gravimetric analysis (TG/DTA) as shown in Fig. 1. The weight losses of the sample have been accomplished stepwise in the temperature range 30-964 °C. Above 964 °C, there was no weight change and the phase formation was completed. This initially provided a precious guidance for choosing proper sintering temperature of this compound. At the first step of the synthesis, a stoichiometric powder mixture of La_2O_3 , NaCl and MnO_2 was assorted competently using ethanol in an agate mortar and then the reactants were dried in an oven in the air atmosphere at 200 °C for 12 h. Then excess NaCl was added as the flux material in 10 times of precursor. Thus the obtained powder calcined at 900 °C for 24 h in an air atmosphere for the flux growth. The crystalline $\text{La}_{0.85}\text{Na}_{0.15}\text{MnO}_3$ sample was obtained in the solid form surrounded by flux material. The flux material was washed by hot water several times and the crystalline $\text{La}_{0.85}\text{Na}_{0.15}\text{MnO}_3$ powder was obtained by filtration. The powder sample was pelletized in 8 mm diameter under pressure of 60 kN using pressure gauge. The temperature rising and cooling rates were 2° C per min. in all the heat treatments procedure.

2.2. Characterization methods

BRUKER D8 advance (Germany) X-ray diffractometer was used to record XRD pattern of $\text{La}_{0.85}\text{Na}_{0.15}\text{MnO}_3$ in the range of diffraction angle (2θ) between 20° and 80° . The X-ray source was Cu-K_α with a voltage of 40 kV and a current of 30 mA. Nicolet-6700 model was used to record Fourier Transform Infrared Spectroscopy (FTIR) measurement of the sample in the wave number range $400\text{--}4000\text{ cm}^{-1}$. UV-Visible spectrometer (Shimadzu UV-1650 PC, Japan) and Agilent Precision Impedance Analyzer (Agilent technologies 4294A, Japan) was used to analyze optical and electrical properties respectively.

3. Results and Discussion

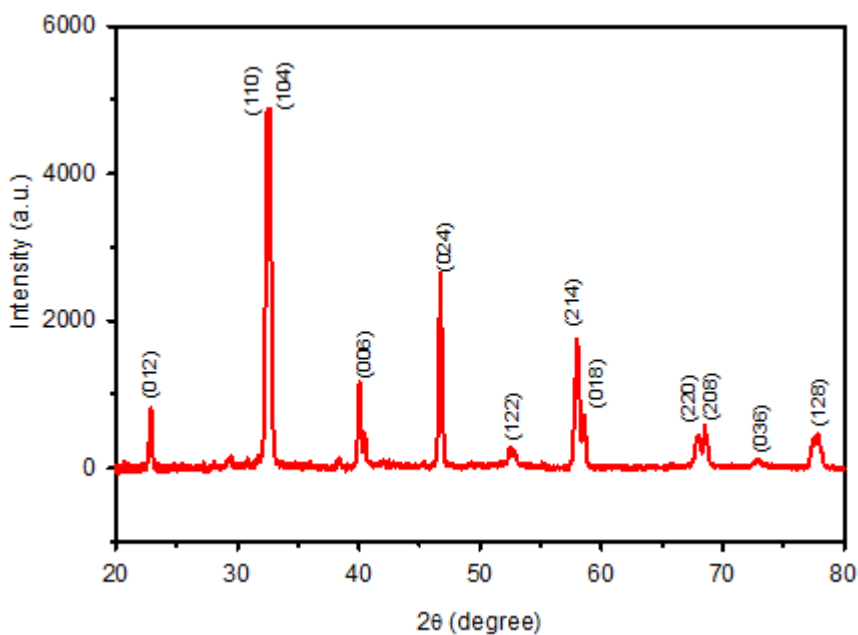


Fig. 2. The X-ray diffraction pattern for the $\text{La}_{0.85}\text{Na}_{0.15}\text{MnO}_3$ sample.

The powder sample was characterized at room temperature by an X-ray diffractometer in the range from $2\theta=20^\circ$ to 80° with CuK_α radiation ($\lambda=1.5418\text{ \AA}$), at 40 kV and 30 mA. Typical XRD pattern for crystalline powder of $\text{La}_{0.85}\text{Na}_{0.15}\text{MnO}_3$ indexing with JCPDS data No. 50-0298 is shown in Fig. 2. Homogeneous rhombohedral perovskites crystal structure of $\text{La}_{0.85}\text{Na}_{0.15}\text{MnO}_3$ sample with the space group of $R\text{-}3c$ has been identified from the XRD spectrum. Using XRD data together with cell cal software the lattice parameters $a=b=5.504\text{ \AA}$, $c=13.37\text{ \AA}$ and unit cell volume 350.89 \AA^3 have been obtained from the refinement of the hexagonal unit cell for the $\text{La}_{0.85}\text{Na}_{0.15}\text{MnO}_3$. These obtained structural parameters are listed in Table 1 and have been compared with the reported data for doping amount $x=0.15$ [13,15]. This comparison reveals that reported values are consistent with the existing literatures. The spectrum clearly shows the diffraction peak at

$2\theta = 22.9^\circ, 32.48^\circ, 32.72^\circ, 40.08^\circ, 46.74^\circ, 52.5^\circ, 58^\circ, 67.98^\circ, 68.54^\circ, 73.08^\circ$ and 77.82° are assigned to (012), (110), (104), (006), (024), (112), (214), (220), (208), (036) and (128) planes respectively of rhombohedral perovskites crystal structure. No impurity phase peaks of La_2O_3 , NaCl and MnO_2 were detected into the entire spectrum for the $\text{La}_{0.85}\text{Na}_{0.15}\text{MnO}_3$ sample reveals the single phase powder was obtained with no impurity. The XRD spectrum shows doublet peaks in the pattern. Splitting of the (110)/(104), (214)/(108) and (220)/(208) doublets near $32.5, 58$ and 68° indicate a highly ordered layered structure for the cathode materials [24]. The average grain size (D) has been calculated using Scherrer formula,

$$D = \frac{0.9\lambda}{\beta \cos\theta} \tag{1}$$

where $0.9, \lambda, \beta$ and θ are indicating the crystal shape constant, X-ray wavelength (1.5418 \AA), full width at half maximum (FWHM) of the highest peak in radians and reflection angle of the highest peak respectively [25,26]. The calculated value of D is found to be 21.29 nm . The value of grain size in the present study is in good agreement with the available experimental data.

Table 1. Structural parameters of $\text{La}_{0.85}\text{Na}_{0.15}\text{MnO}_3$ derived from X-ray diffraction data and comparison with the other reported values for the different synthesis methods for doping amount of $x = 0.15$.

Method of synthesis	Crystal Structure	Lattice Parameters (\AA)	Unit Cell Volume (\AA^3)	Ref.
Chemical Method	Rhombohedral perovskites structure with R-3c space group	$a=b=5.490$ $c=13.30$	346.88	[13]
Solid-State Reaction Method	Rhombohedral perovskites structure with R-3c space group	$a=b=5.5268$ $c=13.357$	407.997	[15]
Flux method	Rhombohedral perovskites structure with R-3c space group	$a=b=5.504$ $c=13.37$	350.89	This work

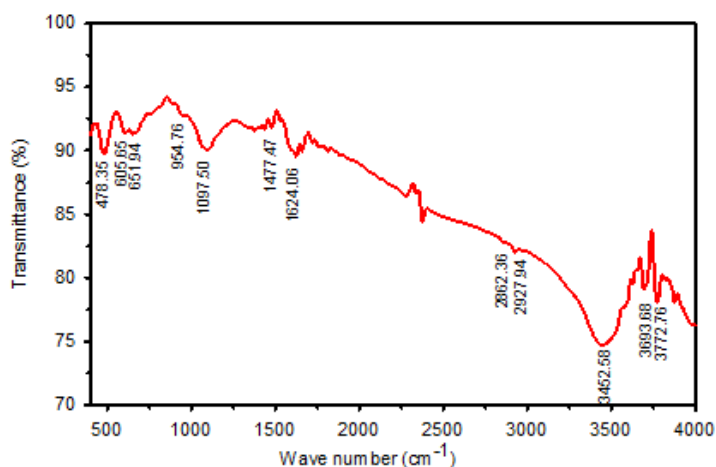


Fig. 3. FTIR spectrum for $\text{La}_{0.85}\text{Na}_{0.15}\text{MnO}_3$ sample.

Fig. 3 shows the FTIR spectrum of $\text{La}_{0.85}\text{Na}_{0.15}\text{MnO}_3$. To identify the functional groups of the active components based on the peak value and to confirm structural formation, we have used the FTIR spectroscopy in the region between 400 cm^{-1} and 4000 cm^{-1} of infrared radiation. The absorption bands of FTIR spectrum located at 478 , 605 and 651 cm^{-1} represent the three characteristics band of $\text{La}_{0.85}\text{Na}_{0.15}\text{MnO}_3$. The absorption peak at 478 cm^{-1} is indicative to the vibration for La-O bond [27]. The absorption band around 605 and 651 cm^{-1} are representing a significant stretching mode of vibration for the Mn-O bond, due to an internal motion of the Mn-ion against the oxygen octahedron and deformation of bound O-Mn-O bond length respectively [28]. This confirms that the vibration bands for precursors vanished and the vibration bands for oxide network developed within the expected perovskites structure.

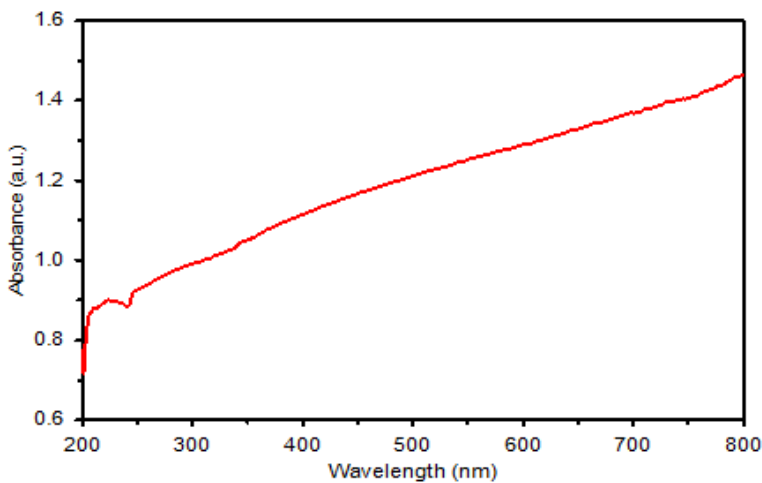


Fig. 4. The UV-visible absorption spectrum for $\text{La}_{0.85}\text{Na}_{0.15}\text{MnO}_3$ sample.

The steep shaped absorption spectrum of $\text{La}_{0.85}\text{Na}_{0.15}\text{MnO}_3$ crystalline powder variation with wavelength from 200 to 800 nm is shown in Fig. 4, which has very similar pattern like Sr-doped lanthanum manganite observed by Turkey *et al.* [29]. The steep shaped absorption spectrum may be originated from the fact that the transition of an excited electron is only possible from valance band to the conduction band located above Fermi level, because of completeness of all the states below the Fermi level with the donor states for $\text{La}_{0.85}\text{Na}_{0.15}\text{MnO}_3$. From the analysis of absorption spectrum, it is clear that there are no remarkable absorption peaks in the entire region of the spectrum unless an appearance of lower UV cutoff near 250 nm. The spectrum distinctly exhibit good optical absorbance of 0.9 from 200 to 300 nm for the $\text{La}_{0.85}\text{Na}_{0.15}\text{MnO}_3$ powder. By increasing the wavelength from 300 nm to higher, the absorbance was increased to 1.4.

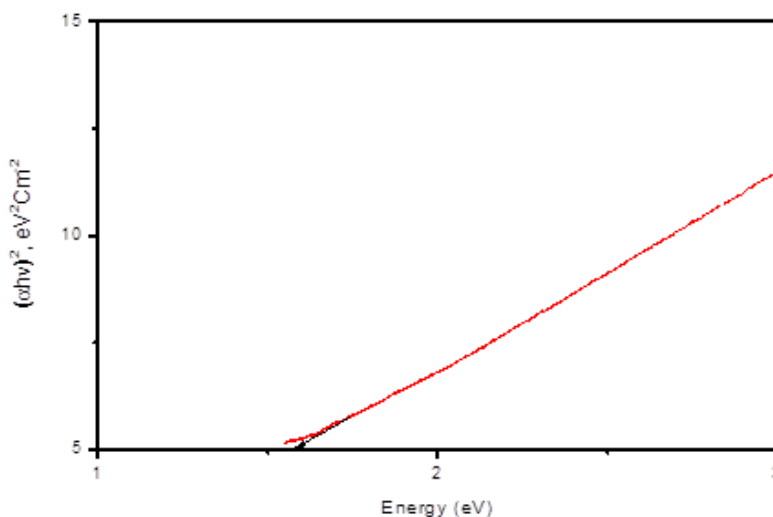


Fig. 5. The optical band gap energy value of the $\text{La}_{0.85}\text{Na}_{0.15}\text{MnO}_3$ powder synthesized using flux method.

Using absorption spectroscopy it is possible to measure the nature of transition whether it direct or indirect band gap semiconductor. Applying Tauc's relation

$$(\alpha h\nu)^m = K(h\nu - E_g) \quad (2)$$

the optical energy band gap (E_g) of $\text{La}_{0.85}\text{Na}_{0.15}\text{MnO}_3$ can be determined by plotting $(\alpha h\nu)^m$ versus photon energy ($h\nu$) curve [30]. Where α is the absorption coefficient and K is a constant. The exponent ' m ' depends on the nature of the optical transition that takes the value of $1/2$, 2 for the indirect-allowed and direct allowed transitions respectively. If the obtained plot diagram is a straight line for $m=1/2$, then the transition is indirect and if it is straight line for $m=2$ then the transition is direct. The energy band gap can be calculated by extrapolating the straight line in to the, $\alpha = 0$ axis [31]. The best linear relation of $(\alpha h\nu)^m$ vs $h\nu$ was determined for $m=2$, indicating that this is a direct allowed electronic transition as shown in Fig. 5. The band gap of the $\text{La}_{0.85}\text{Na}_{0.15}\text{MnO}_3$ is calculated to be about 1.57 eV. This observed energy band gap value is relatively lower for monovalent Na doping than divalent Sr doping in LaMnO_3 , reported in the previously available literature [29,32]. This is due to the fact that there is an increased difference in potential between the Na and La sites due to the large valency difference between Na^+ and La^{3+} ions than the Sr^{2+} and La^{3+} ion [10]. As a consequence more conversion of Mn^{3+} to Mn^{4+} , i.e. larger density of charge carriers are achieved for every amount of Na doping than Sr doping governed by the formula $\text{La}_{(1-x)}^{3+}\text{Na}_{(x)}^+\text{Mn}_{(1-x)}^{3+}\text{Mn}_{(x)}^{4+}\text{O}_3$. The efficiency of solar cell device manifested by the photon to electron conversion [33] and sensitivity of the photosensor highly depends on the absorption capability of the photon. The major limitation for the most common solar cell material 'Si' is indirect band gap, therefore cannot absorb light very well. Several methods and technique [34,35] need to trap the

photon and in some cases, Si-based photovoltaic devices with a thickness less than several micrometers cannot completely absorb photons with the wavelength greater than 600 nm [36]. Hence, higher optical absorbance in the ultra-violet and visible region in addition to enhanced conductivity in semiconducting features of this material can be very effective in photovoltaic devices and thus can initiate a possibility of using $\text{La}_{0.85}\text{Na}_{0.15}\text{MnO}_3$ as photosensor device materials and solar cell fabrications. Moreover, for optical device applications, where absorbance of visible light is required $\text{La}_{0.85}\text{Na}_{0.15}\text{MnO}_3$ can be a good candidate. Several important characteristics of $\text{La}_{0.85}\text{Na}_{0.15}\text{MnO}_3$ such as refractive index (n) and the static dielectric constant (ϵ_0) of the samples have been calculated using the relations

$$E_g n^4 = 95 \text{ eV} \quad (3)$$

$$\epsilon_0 = 18.52 - 3.08 E_g \quad (4)$$

respectively and listed in Table 2 [29,37]. The obtained results have been compared with the Sr-doped lanthanum manganite. This comparison reveals that obtained results are consistent with the Sr-doped lanthanum manganite system [29].

Table 2. Optical band gap, refractive index, high frequency dielectric constant and static dielectric constant for Na and Sr doped lanthanum manganite sample.

Parameters	For Na doping [Present study]	For Sr doping [Ref. 29]
Band gap, E_g (eV)	1.57	1.95
Refractive index, n	2.79	2.73
Static dielectric constant, ϵ_0	7.784	12.46

The ac conductivity of the sample has been measured by impedance analyzer at room temperature, where the signal frequency has been varied from 100 Hz to 10 MHz with the applied oscillating voltage of 300 mV. Fig. 6 shows the frequency dependent ac conductivity of $\text{La}_{0.85}\text{Na}_{0.15}\text{MnO}_3$ sample, where conductivity increases with the increment of frequency. The increased ac-conductivity with the increase of frequency can initiate a better performance of $\text{La}_{0.85}\text{Na}_{0.15}\text{MnO}_3$ in various high-frequency electrical device applications.

The dielectric properties are the measure of material's ability to store electric charge of a material and an important factor in electronic device applications. Dielectric properties of the $\text{La}_{0.85}\text{Na}_{0.15}\text{MnO}_3$ sample have been measured by precision impedance analyzer at room temperature in the range between 100 Hz to 10 MHz. Fig. 7 shows the frequency dependent dielectric constant of $\text{La}_{0.85}\text{Na}_{0.15}\text{MnO}_3$ sample. It can be observed from Fig. 7, that dielectric constant of $\text{La}_{0.85}\text{Na}_{0.15}\text{MnO}_3$ sample is maximum at low frequency due to the bulk polarization of the sample and decrease with the increase of the frequency. The dielectric constant at high frequency comes from the grains which have a small resistance and at low frequency comes from the grains which have a high resistance at the grain boundary region due to voids, dislocations and defects etc. [38,39]. Furthermore, there is a huge influence of Percentage of Relative Humidity (%RH) on the capacitance and

dielectric constants of a material. Q. Zafar *et al.* [40] have shown that with the increase of %RH, capacitance and dielectric constant of a material increase significantly and the influence of %RH variation on dielectric constants and capacitance is stronger in low frequency region compared to the high frequency [41-43]. Consequently, dielectric constant and capacitance of a material decrease with increase in frequency. Fig. 7 also reveals that this material has dielectric response even at zero frequency and the value of static dielectric constant $\epsilon(0)$ is approximately equal to one which is consistent with the predicted value by equation 4. Low dielectric constant material throughout the large frequency range is an important component of microelectronic devices. For ultra-large-scale integration of integrated circuit, several limiting factors are interconnected with dielectric constant and meanwhile replacement of silicon dioxide is being done by low dielectric constant materials [44]. Hence, our material has a great chance to be applied for these purposes.

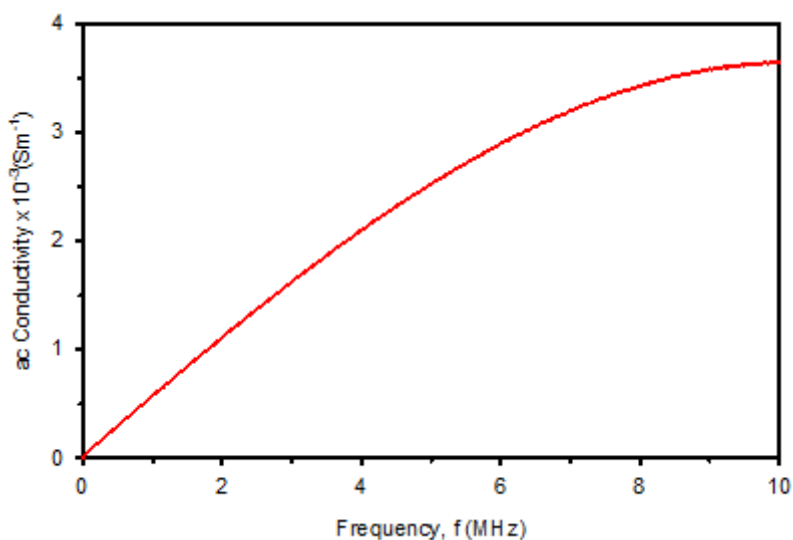


Fig. 6. The frequency dependence ac conductivity $\text{La}_{0.85}\text{Na}_{0.15}\text{MnO}_3$ sample.

The frequency dependent capacitance of $\text{La}_{0.85}\text{Na}_{0.15}\text{MnO}_3$ sample is shown in Fig. 8. The capacitance of $\text{La}_{0.85}\text{Na}_{0.15}\text{MnO}_3$ is high at low-frequency region and decrease with the increase of frequency. At present days ceramic capacitors with values from a few Pico farads to 1 microfarad are used in high-frequency range for compensation of dielectric loss in the audio circuit and these types of capacitors have applications both in electrical and electronic devices [45]. These types of capacitors have applications both in electrical and electronic devices. Hence, capacitor made by $\text{La}_{0.85}\text{Na}_{0.15}\text{MnO}_3$ with capacitance in Pico farad range can be used in filter applications, energy storage systems, motor starters and signal processing devices. Furthermore, for the devices, where the capacitance is

required to stay nearly stable above a certain value of frequency $\text{La}_{0.85}\text{Na}_{0.15}\text{MnO}_3$ system can be chosen.

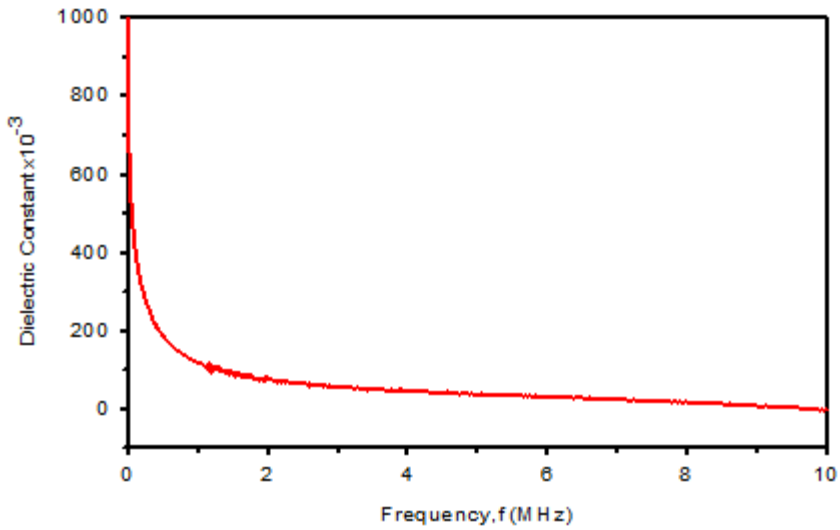


Fig. 7. The frequency dependence dielectric constant of $\text{La}_{0.85}\text{Na}_{0.15}\text{MnO}_3$ sample.

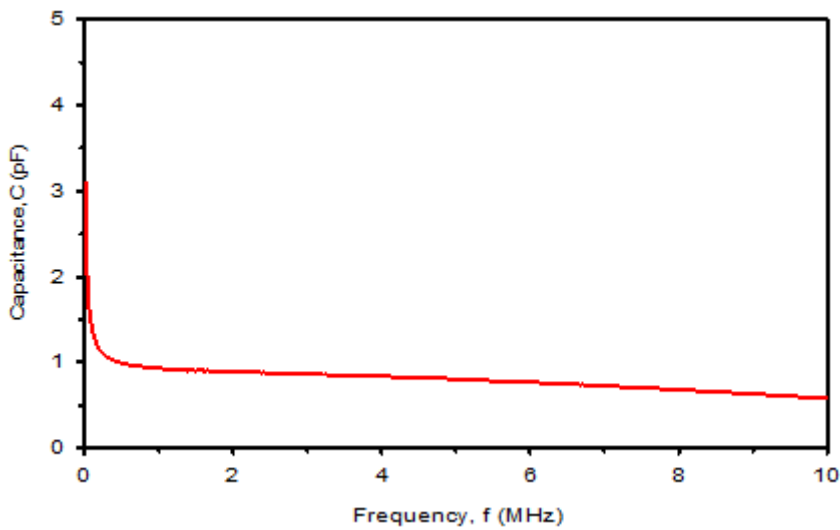


Fig. 8. The frequency dependence capacitance of $\text{La}_{0.85}\text{Na}_{0.15}\text{MnO}_3$ sample.

4. Conclusion

The addition of salt flux with the conventional solid-state reaction was satisfactory to produce homogeneous single phasic crystal structure with no impurity phase peaks. In case of optical properties, we found better optical absorbance for monovalent Na doping with slightly lower value of energy band gap than divalent Sr doping. The ac conductivity increases with frequency for Na-doped sample. The dielectric constant decreases rapidly with increasing frequency and then reaches a constant value. Low dielectric constants at high-frequency are very effective for high-frequency application in electrical circuits to minimize dielectric losses. All these observed properties might be improved more by choosing suitable monovalent metal (Li, K, etc.) substitution with a proper doping content, will be studied in our next attempt.

Acknowledgments

This work was partially supported by the Khulna University Research Cell (Khubi/Gacell-04/2000-13). Authors would like to thank Khulna University authority for providing funds under the university research project to carry out this work. The authors like to thank K. Hoque, Physics Discipline, Khulna University and M. K. Amin, Chemistry Discipline, Khulna University for their cooperation and suggestion during this research work.

References

1. M. Mori, Y. Hiei, N. M. Sammes, and G. A. Tompsett, *J. Electrochem. Soc.* **147**, 1295 (2000). <https://doi.org/10.1149/1.1393353>
2. *Colossal Magneto-Resistive Oxides*, ed. T. Tokura (Gordon and Breach Science Publishers, New York, 2000).
3. J. F. Mitchell, D. N. Argyriou, C. D. Potter, D. G. Hinks, J. D. Jorgensen, and S. D. Bader, *Phys. Rev. B* **54**, 6172 (1996). <https://doi.org/10.1103/PhysRevB.54.6172>
4. T. Li, B. Wang, H. Dai, Y. Du, H. Yan, and Y. Liu, *J. Appl. Phys.* **98**, 123505 (2005). <https://doi.org/10.1063/1.2042528>
5. J. Mizusaki, H. Tagawa, K. Naraya, and T. Sasamoto, *Solid State Ionics*, **49**, 111 (1991). [https://doi.org/10.1016/0167-2738\(91\)90076-N](https://doi.org/10.1016/0167-2738(91)90076-N)
6. A. O. Isenberg – *Proc. High Temperature Solid Oxide Electrolyte* (Brookhaven National Laboratory, Publ. BNL 51728, 1983), p.4.
7. A. J. Millis, P. B. Littlewood, and B. I. Shraiman, *Phys. Rev. Lett.* **74**, 5144 (1995). <https://doi.org/10.1103/PhysRevLett.74.5144>
8. C. H. Chen and S-W. Cheong, *Phys. Rev. Lett.* **76**, 4042 (1996). <https://doi.org/10.1103/PhysRevLett.76.4042>
9. Y. Takeda, Y. Sakaki, T. Ichikawa, N. Imanishi, O. Yamamoto, M. Mori, N. Mori, and T. Abe, *Solid State Ionics* **72**, 257 (1994). [https://doi.org/10.1016/0167-2738\(94\)90156-2](https://doi.org/10.1016/0167-2738(94)90156-2)
10. S. Roy, Y. Q. Guo, S. Venkatesh, and N. Ali, *J. Phys.: Condens. Matter* **13**, 9547 (2001). <https://doi.org/10.1088/0953-8984/13/42/314>
11. G. H. Rao, J. R. Sun, K. Barner, and N. Hamad, *J. Phys.: Condens. Matter* **11**, 1523 (1999). <https://doi.org/10.1088/0953-8984/11/6/016>
12. C. O. Ehi-Eromosele, B. I. Ita, K. O. Ajanaku, A. Edobor-Osoh, O. Aladesuyi, S. A. Adalikwu, and F. E. Ehi-Eromosele, *Bull. Mater. Sci.* **38**, 1749 (2015). <https://doi.org/10.1007/s12034-015-1046-1>

13. Y. K. Lakshmi, G. Venkataiah, and P. Venugopal Reddy, *J. Appl. Phys.* **106**, 023707 (2009).
<https://doi.org/10.1063/1.3173285>
14. L. Malavasi, M. C. Mozzati, S. Polizzi, C. B. Azzoni, and G. Flor, *Chem. Mater.* **15**, 5036 (2003). <https://doi.org/10.1021/cm0311271>
15. S. B. Kansara, D. Dhruva, B. Kataria, C. M. Thaker, S. Rayaprol, C. L. Prajapat, M. R. Singhc, P. S. Solanki, D. G. Kuberkar, and N. A. Shaha, *Ceram. Int.* **41**, 7162 (2015).
<https://doi.org/10.1016/j.ceramint.2015.02.037>
16. L. Malavasi, M. C. Mozzati, P. Ghigna, C. B. Azzoni, and G. Flor, *J. Phys. Chem. B* **107**, 2500 (2003). <https://doi.org/10.1021/jp027015z>
17. A. M. Haghiri-Gosnet, and J. P. Renard, *J. Phys. D: Appl. Phys.* **36**, R127 (2003).
<https://doi.org/10.1088/0022-3727/36/8/201>
18. C. Zener, *Phys. Rev.* **81**, 440 (1951). <https://doi.org/10.1103/PhysRev.81.440>
19. C. Mitra, R. Pinto, A. K. Nigam, and S. K. Dhar, *Appl. Phys. Lett.* **79**, 2408 (2001).
<https://doi.org/10.1063/1.1409592>
20. T. C. Ozawa and S. M. Kauzlarich, *Inorg. Chem.* **42**, 3183 (2003).
<https://doi.org/10.1021/ic034061k>
21. M. Brylak, M. H. Möller, and W. J. Jeitschko, *Solid State Chem.* **115**, 305 (1995).
<https://doi.org/10.1006/jssc.1995.1138>
22. A.T. Nientiedt, W. Jeitschko, P. G. Pollmeier, and M. Z. Brylak, *Zeitschrift Fur Naturforschung B.* **52**, 560 (1997). <https://doi.org/10.1515/znb-1997-0504>
23. A.T. Nientiedt and W. Jeitschko, *Inorg. Chem.* **37**, 386 (1998).
<https://doi.org/10.1021/ic971058q>
24. P. Xiao, T. J. Lv, X. Chen, and C. Chang, *Sci. Rep.* **7**, 1408 (2017).
<https://doi.org/10.1038/s41598-017-16078-x>
25. K. Rajasekar, L. Kungumadevi, L. Subbarayan, and R. Sathyamoorthy, *Ionics* **14**, 69 (2008).
<https://doi.org/10.1007/s11581-007-0146-3>
26. M. Yilmaz, G. Turgut, and S. Aydin, *J. Chem. Soc. Pak.* **34**, 283 (2012).
27. D. Berger, N. Van Landschot, C. Ionica, F. Papa, and V. Fruth, *J. Optoelectron. Adv. Mater.* **5**, 719 (2003).
28. K. H. Kim, J. Y. Gu, H. S. Choi, G. W. Park, and T. W. Noh, *Phys. Rev. Lett.* **77**, 1877 (1996).
<https://doi.org/10.1103/PhysRevLett.77.207>
29. A. O. Turkey, M. M. Rashad, A. M. Hassan, E. M. Elnaggar, and M. Bechelany, *Phys. Chem. Chem. Phys.* **19**, 6878 (2017). <https://doi.org/10.1039/C6CP07333F>
30. A. O. Turkey, M. M. Rashad, and M. Bechelany, *Mater. Des.* **90**, 54 (2016).
<https://doi.org/10.1016/j.matdes.2015.10.113>
31. J. I. Pankove, *Optical Process in Semiconductor* (Dover, New York, 1971).
32. M. Cesaria, A. P. Caricato, G. Leggieri, M. Martino, and G. Maruccio, *Thin Solid Films* **545**, 592 (2013). <https://doi.org/10.1016/j.tsf.2013.07.071>
33. S. M. Sze and K. K. Ng, *Physics of Semiconductor Devices* (Wiley, Hoboken, NJ, USA, 2007).
34. E. Yablonovitch and G. D. Cody, *IEEE Trans. Electron. Dev.* **29**, 300 (1982).
<https://doi.org/10.1109/T-ED.1982.20700>
35. H. W. Deckman, C. B. Roxlo, and E. Yablonovitch, *Opt. Lett.* **8**, 491 (1983).
<https://doi.org/10.1364/OL.8.000491>
36. Y. Tanaka, Y. Kawamoto, M. Fujit, and S. Noda, *Opt. Express* **21**, 20112 (2013).
<https://doi.org/10.1364/OE.21.20111>
37. T. S. Moss, *Phy. Stat. Sol. B* **131**, 415 (1985).
38. M. Raghavudha, D. Ravinder, and P. Veerasomaiah, *Mat. Sc. Applicat.* **4**, 7 (2013).
<https://doi.org/10.4236/msa.2013.47052>
39. J. Tasawar, M. Asghari, and A. M. Akhlaq J. *Supercond. Nov. Magn.* **24**, 2137 (2011).
<https://doi.org/10.1007/s10948-011-1168-7>
40. P. S. Ho, J. Leu, and W. W. Lee, *Low Dielectric Constant Materials for IC Applications* (Springer-Verlag, Berlin Heidelberg, 2003). <https://doi.org/10.1007/978-3-642-55908-2>

41. Q. Zafar and K. Sulaiman *React. Funct. Polym.* **105**, 45 (2016).
<https://doi.org/10.1016/j.reactfunctpolym.2016.05.014>
42. Q. Zafar, M. I. Azmer, K. Sulaiman, M. S. Al-Assiri A. G. Al-Sehemi, and A. Kalam, *J. Nanopart. Res.* **18**, 186 (2016). <https://doi.org/10.1007/s11051-016-3488-9>
43. A. G. Al-Sehemi, M S. Al-Assiri, Abul Kalama, Q. Zafar, M. I. Azmer, K. Sulaimanf, and Z. Ahmad, *Sensors and Actuators B*, **231**, 30 (2016). <https://doi.org/10.1016/j.snb.2016.03.004>
44. S. B. Aziz, W. O. Karim, K. W. Quadir, and Q. Zafar, *Int. J. Electrochem. Sci.* **13**, 6112 (2018). <https://doi.org/10.20964/2018.06.38>
45. Capacitors-types-applications. Available: www.elprocus.com (accessed on 7 May 2018).